

# TOOL-HOLDER CONNECTION MODELING FOR FREQUENCY RESPONSE PREDICTION IN MILLING

Kevin B. Powell, Dongki Won, Tony L. Schmitz, G. Scott Duncan, W. Gregory Sawyer, John C. Ziegert  
 Department of Mechanical and Aerospace Engineering  
 University of Florida  
 Gainesville, FL, USA

## INTRODUCTION

Discrete part production by milling is an important manufacturing capability. However, there are many potential obstacles to producing quality parts at low cost in a timely manner. One particular limitation that has received considerable attention in the literature is chatter, or unstable machining; a second is surface location error, or an error in the part dimension caused by dynamic deflections of the tool (and potentially the part/fixture) during stable cutting. In both cases, a primary factor affecting the process performance is the system frequency response function, or FRF.

The system FRF, often dominated by the flexibility of the tool-holder-spindle assembly as reflected at the tool's free end, can be obtained using impact testing, where an instrumented hammer is used to excite the tool at its free end (i.e., the tool point) and the resulting vibration is measured using an appropriate transducer. However, due to the large number of spindle, holder, and tool combinations that may be available in a particular production facility, the required testing time can be significant. Further, the measured response is often strongly dependent on the tool overhang length. Therefore, a model which is able to predict the tool point response based on minimum input data is the preferred alternative.

The purpose of this paper is to build on the previous work of Schmitz *et al.* [1-3], which describes tool point FRF, or receptance, prediction using the Receptance Coupling Substructure Analysis (RCSA) method. In these previous studies, two and three component models of the machine-spindle-holder-tool assembly were defined. In this work, we extend the three component model to include multiple connections between the tool and holder along the interference contact within the (thermal) shrink fit holder. This is shown schematically in Fig. 1, where multiple complex stiffness

matrices,  $K_i$ , describe the connection parameters at each location. In this new model the fully populated  $K$  matrix is defined as shown in Eq. 1, which accounts for the displacement imposed by moment and the rotation caused by force through the non-zero off diagonal terms. Finite element models are developed to determine the position-dependent stiffness and equivalent viscous damping values for a thermal shrink fit connection between the tool and holder, which represents the preferred interface for high-speed milling applications. Using these values, the tool point FRF is predicted *a priori* and compared to measurements.

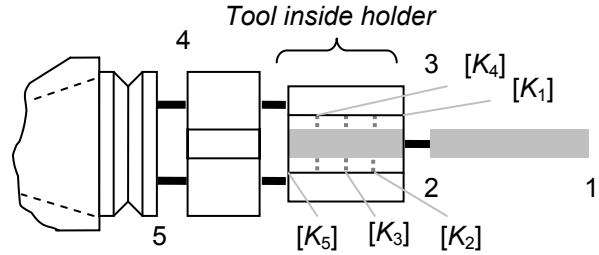


Figure 1. Three component RCSA model – the finite stiffness/damping between the tool and holder is represented by multiple  $K$  matrices determined from finite element simulation.

$$K = \begin{bmatrix} k_{yf} + i\omega \cdot c_{yf} & k_{ym} + i\omega \cdot c_{ym} \\ k_{\theta f} + i\omega \cdot c_{\theta f} & k_{\theta m} + i\omega \cdot c_{\theta m} \end{bmatrix} \quad (1)$$

## RCSA MODEL

The RCSA spindle-holder-tool model is composed of three components. The spindle response is obtained by inserting a standard geometry artifact in the spindle and recording one direct and one cross FRF on the artifact. Using this data, together with a model of the artifact, the spindle receptances may be obtained by decoupling the artifact response from the spindle [3]. As shown in Fig. 1, the holder is separated into two sections: the portion with the tool inserted and the remainder of the

holder. In this work, we couple the portion of the tool inside the holder to the holder through multiple damped springs to capture the non-rigid behavior of the shrink fit connection. Finally, the portion of the tool outside the holder is rigidly coupled to the holder and spindle to predict the tool point FRF.

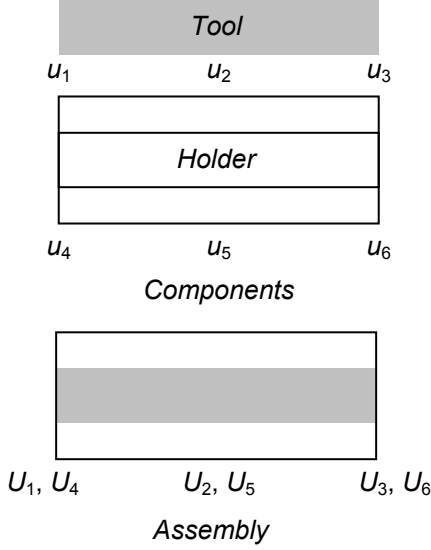


Figure 2. Tool-in-holder coordinates.

To demonstrate the coupling between the concentric inner tool and outer holder components, the case of  $n = 3$  connection coordinates, located at the ends of the contact length and at the mid-point, is now presented. The portions of the tool and holder in shrink fit contact are treated as free-free beams. For  $n = 3$ , a total of six component coordinates is obtained – three each on the internal tool and external holder (see Fig. 2) [4]. The component displacement/rotations can be written as shown.

$$\begin{aligned}
 u_1 &= R_{11}q_1 + R_{12}q_2 + R_{13}q_3 \\
 u_2 &= R_{21}q_1 + R_{22}q_2 + R_{23}q_3 \\
 u_3 &= R_{31}q_1 + R_{32}q_2 + R_{33}q_3 \\
 u_4 &= R_{44}q_4 + R_{45}q_5 + R_{46}q_6 \\
 u_5 &= R_{54}q_4 + R_{55}q_5 + R_{56}q_6 \\
 u_6 &= R_{64}q_4 + R_{65}q_5 + R_{66}q_6
 \end{aligned} \quad (2)$$

Here, the component displacements/rotations, forces/moments, and receptances are  $u_i = \{y_i \ \theta_i\}^T$ ,  $q_i = \{f_i \ m_i\}^T$ , and,

$$R_{ij}(\omega) = \begin{bmatrix} \frac{y_i}{f_j} & \frac{y_i}{m_j} \\ \frac{\theta_i}{f_j} & \frac{\theta_i}{m_j} \end{bmatrix} = \begin{bmatrix} h_{ij} & l_{ij} \\ n_{ij} & p_{ij} \end{bmatrix}$$

respectively. The compatibility conditions for the flexible/damped shrink fit connection are:

$$\begin{aligned}
 K_1(u_4 - u_1) &= -q_4, \quad K_2(u_5 - u_2) = -q_5, \quad \text{and,} \\
 K_3(u_6 - u_3) &= -q_6,
 \end{aligned} \quad (3)$$

where  $K_i$  is given by Eq. 1 and the component and assembly coordinates are defined at the same spatial locations so that  $u_i = U_i$ ,  $i = 1$  to 6. If the assembly direct response at the left end,  $G_{11}(\omega)$ , is to be determined,  $Q_1$  is applied to coordinate  $U_1$  of the assembly (the upper case variables denote assembly coordinates, forces, and moments). The equilibrium conditions are then  $q_1 + q_4 = Q_1$ ,  $q_2 + q_5 = 0$ , and  $q_3 + q_6 = 0$ .

$G_{11}$  is determined in steps using the relevant equations. The first step is to insert the component displacement/rotation expressions into the compatibility conditions. The next step is to substitute  $q_4 = Q_1 - q_1$ ,  $q_5 = -q_2$ , and  $q_6 = -q_3$  and rearrange to obtain:

$$\begin{bmatrix} R_{11} + R_{44} + K_1^{-1} & R_{12} + R_{45} & R_{13} + R_{46} \\ R_{21} + R_{54} & R_{22} + R_{55} + K_2^{-1} & R_{23} + R_{54} \\ R_{31} + R_{64} & R_{32} + R_{65} & R_{33} + R_{66} + K_3^{-1} \end{bmatrix} \cdot \begin{Bmatrix} q_1 \\ q_2 \\ q_3 \end{Bmatrix} = Q_1 \begin{bmatrix} R_{44} + K_1^{-1} \\ R_{54} \\ R_{64} \end{bmatrix}$$

which gives the relationship between the component forces/moments and externally applied force/moment.  $G_{11}$  can be expressed as:

$$G_{11} = \frac{U_1}{Q_1} = \frac{u_1}{Q_1} = R_{11} \frac{q_1}{Q_1} + R_{12} \frac{q_2}{Q_1} + R_{13} \frac{q_3}{Q_1}, \quad (4)$$

so the ratios  $\frac{q_1}{Q_1}$ ,  $\frac{q_2}{Q_1}$ , and  $\frac{q_3}{Q_1}$  are required.

These can be determined from:

$$\frac{1}{Q_1} \begin{Bmatrix} q_1 \\ q_2 \\ q_3 \end{Bmatrix} = \begin{bmatrix} R_{11} + R_{44} + K_1^{-1} & R_{12} + R_{45} & R_{13} + R_{46} \\ R_{21} + R_{54} & R_{22} + R_{55} + K_2^{-1} & R_{23} + R_{54} \\ R_{31} + R_{64} & R_{32} + R_{65} & R_{33} + R_{66} + K_3^{-1} \end{bmatrix}^{-1} \cdot \begin{bmatrix} R_{44} + K_1^{-1} \\ R_{54} \\ R_{64} \end{bmatrix} = [A]$$

where  $[A]$  is a 6 by 2, or  $2n$  by 2, by  $N$  matrix ( $N$  is the number of points in the frequency vector,  $\omega$ ). The reader may note that the matrix size is 6 by 2 because  $R_{ij}$  is a 2 by 2 matrix. The matrix  $A$  is partitioned as follows: the first two rows of  $A$

give  $\frac{q_1}{Q_1}$ ; the second two rows provide  $\frac{q_2}{Q_1}$ ; and

the final two rows give  $\frac{q_3}{Q_1}$ . The desired direct

receptances can then be computed from Eq. 4. This 3-point coupling example can be extended to  $n$  coupling points by recognizing the recursive pattern in  $[A]$ .

Once the shrink fit connection stiffness is incorporated into the tool-holder assembly as defined in the next section, the remaining components can be rigidly coupled. Assembly coordinate definitions for the overhung portion of the tool (1-2), extended holder (3-4), and spindle-holder base (5) are shown in Fig. 1. The corresponding RCSA equation for the assembly receptances at the tool point is obtained by: 1) rigidly coupling the overhung free-free tool to the free-free tool-extended holder to determine the new subassembly direct receptances at each end,  $GS_{11}$  and  $GS_{44}$ , and the cross receptances,  $GS_{14}$  and  $GS_{41}$ ; and 2) using the standard holder and finite difference calculations to determine the four receptances at the free end of the standard holder, removing the portion of the standard holder beyond the flange using inverse RCSA, and defining the direct receptance at the free end of the spindle-holder subassembly,  $GS_{55}$ . See the next equation, where

$H_{11}(\omega) = \frac{Y_1}{F_1}$  is the FRF generally required for

milling stability and surface location error analyses. Additional details are available in references [3-4].

$$G_{11} = \begin{bmatrix} H_{11} & L_{11} \\ N_{11} & P_{11} \end{bmatrix} = GS_{11} - GS_{14}(GS_{44} + GS_{55})^{-1}GS_{41}$$

## FINITE ELEMENT MODEL

A model for a 19.1 mm diameter carbide tool blank inserted in a steel tapered shrink fit holder was developed using ANSYS. The boundary conditions were set as fixed-free and only the extended holder and tool were modeled. In this example, 6324 20-node cubic elements (SOLID184), 768 8-node contact elements (CONTA174), and 768 8-node target elements (TARGE170) were applied, where the flexible-to-flexible contact/target elements were located at the interface between the tool and holder. The coordinate directions for the model were:  $x$  – horizontal,  $y$  – vertical,  $z$  – along the tool axis.

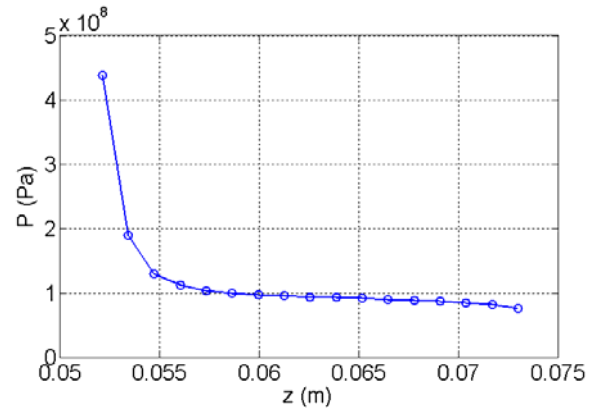


Figure 3. Simulated contact pressure profile for the shrink fit tool-holder interface (10  $\mu\text{m}$  radial interference). The  $z$  axis origin was located at the fixed end of the holder.

The finite element simulations were carried out in two primary time intervals. In the first interval, the contact pressure between the tool and holder was allowed to grow due to the imposed radial interference. Figure 3 shows the simulated contact pressure,  $P$ , profile for the model with a 10  $\mu\text{m}$  radial interference. In the second interval, the  $y$  direction force or couple was applied to the tool just beyond the end of contact. The forces were applied using an equivalent nodal force arrangement (to minimize localized deformation effects). For both intervals, time was divided into five equal steps.

The position-dependent stiffness values were determined using the following steps. At the end of the two time intervals, the  $y$  direction displacements of the tool at nodes along the tool

top centerline were recorded. The  $y$  displacements, as a function of  $z$  location, imposed by the force/couple were then computed by differencing the two results. By applying a range of forces and couples, the  $k_{yf}(z)$  and  $k_{ym}(z)$  stiffness values from Eq. 1 were calculated directly from the slope of the load-displacement curves for each node under consideration. For the  $k_{of}(z)$  and  $k_{om}(z)$  stiffness values, the rotation was first calculated by central finite difference from the displacement data, then the stiffness values were obtained from the load-rotation curve slope values. Example results for the  $k_{yf}(z)$  values are provided in Fig. 4.

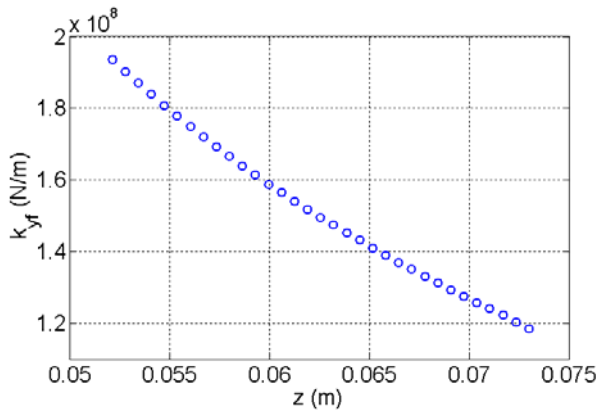


Figure 4. Stiffness values for the finite element model (10  $\mu$ m radial interference).

It was assumed that energy dissipation in the shrink fit connection occurred due to relative micro-slip between the tool and holder along the tool axis during the force/couple application. This Coulomb damping was converted to position-dependent equivalent viscous damping values by: 1) computing the friction (damping) force,  $F_d$ , for each element,  $n$ ; 2) calculating the viscous damping value for each element

according to  $c_{eq,n} = \frac{4F_{d,n}}{\pi\omega \cdot |z_n|}$  [6], where  $|z_n|$  is

the absolute value of the contact element displacement along the tool axis; and 3) summing the damping values for the elements located around the tool circumference for the selected  $z$  location.

## RESULTS

To test the approach, thirty 19.1 mm diameter carbide tool blanks were sequentially inserted in the modeled holder and the tool point FRF was recorded. The insertion length was maintained

at 22.9 mm while the overhang length varied from {66.0 to 142.2} mm. A comparison of the measurements and predictions is shown in Fig. 5. The top and middle panels show the measurements and predictions (same scale). The bottom panel shows the percent difference between the measured and predicted (dominant) natural frequencies as a function of the tool overhang length. Agreement of 2% or better is observed for all cases.

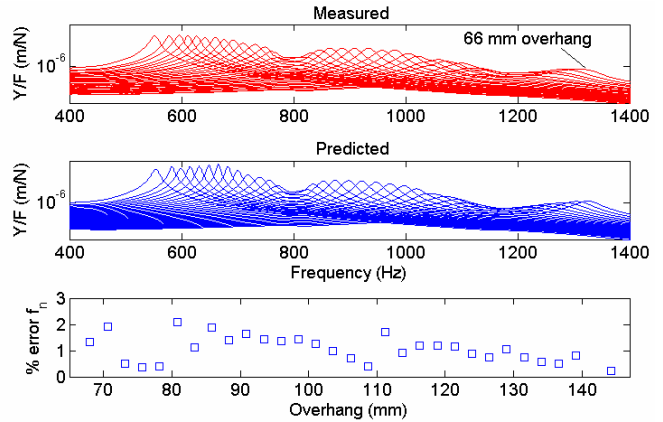


Figure 5. Top – measured FRF magnitudes; middle – predicted magnitudes; and bottom – percent difference between measured and predicted (dominant) natural frequencies,  $f_n$ .

## ACKNOWLEDGEMENTS

This work was supported by the National Science Foundation (DMI-0238019), the Office of Naval Research, and TechSolve. The three-component RCSA approach is patent-pending.

## REFERENCES

- Schmitz, T. and Donaldson, R., 2000, Predicting High-Speed Machining Dynamics by Substructure Analysis; *Annals of the CIRP*, 49/1: 303-308.
- Schmitz, T., Davies, M., and Kennedy, M., 2001, Tool Point Frequency Response Prediction for High-Speed Machining by RCSA, *Journal of Manufacturing Science and Engineering*, 123: 700-707.
- Schmitz, T. and Duncan, G.S., 2005, Three-Component Receptance Coupling Substructure Analysis for Tool Point Dynamics Prediction; *Journal of Manufacturing Science and Engineering*, 127/4: 781-790.
- Schmitz, T., Duncan, G.S., 2006, Receptance Coupling for Dynamics Prediction of Assemblies with Coincident Neutral Axes, *Journal of Sound and Vibration*, 289/4-5: 1045-1065.
- Thomson, W. and Dahleh, M., 1998, *Theory of Vibration with Applications*, 5<sup>th</sup> Edition, Prentice Hall, Upper Saddle River, NJ.